Two-phase dynamics of p53 in the DNA damage response

Xiao-Peng Zhang, Feng Liu[1], and Wei Wang[1]

National Laboratory of Solid State Microstructures and Department of Physics, Nanjing University, Nanjing 210093, China

Edited* by José N. Onuchic, University of California, La Jolla, CA, and approved April 21, 2011 (received for review January 12, 2011)

The tumor suppressor p53 mainly induces cell cycle arrest/DNA repair or apoptosis in the DNA damage response. How to choose between these two outcomes is not fully understood. We proposed a four-module model of the p53 signaling network and associated the network dynamics with cellular outcomes after ionizing radiation. We found that the cellular response is mediated by both the level and posttranslational modifications of p53 and that p53 is activated in a progressive manner. First, p53 is partially activated by primary modifications such as phosphorylation at Ser-15/20 to induce cell cycle arrest, with its level varying in a series of pulses. If the damage cannot be fixed after a critical number of p53 pulses, then p53 is fully activated by further modifications such as phosphorylation at Ser-46 to trigger apoptosis, with its concentration switching to rather high levels. Thus, p53 undergoes a two-phase response in irreparably damaged cells. Such combinations of pulsatile and switch-like behaviors of p53 may represent a flexible and efficient control mode, avoiding the premature apoptosis and promoting the execution of apoptosis. In our model, p53 pulses are recurrently driven by ataxia telangiectasia mutated (ATM) pulses triggered by DNA damage. The p53-Mdm2 and ATM-p53-Wip1 negative feedback loops are responsible for p53 pulses, whereas the switching behavior occurs when the p53-PTEN-Akt-Mdm2 positive feedback loop becomes dominant. Our results suggest that a sequential predominance of distinct feedback loops may elicit multiple-phase dynamical behaviors. This work provides a new mechanism for p53 dynamics and cell fate decision.

bistability | digital mode | signal transduction | numerical simulations

The tumor suppressor p53 is at the hub of cellular signaling networks that are activated by stress signals including DNA damage (1). In unstressed cells, p53 is kept at low levels by its negative regulator Mdm2 (2). Upon DNA damage, p53 is stabilized and activated to function primarily as a transcription factor, regulating expression of downstream target genes. This leads to different cellular outcomes such as cell cycle arrest and apoptosis (3); the former facilitates DNA repair and promotes cell survival, whereas the latter provides an efficient way to remove irreparably damaged cells. However, the mechanism for p53-mediated cell fate decision between life and death is not fully understood.

It is known that p53 responds to DNA damage in various modes, depending on cell and stress types (1). Previously, it was proposed that low levels of p53 induce cell cycle arrest, whereas high levels of p53 induce apoptosis (4). Such an analog mode is consistent with the fact that p53 binds to proarrest genes with high affinities but associates with proapoptotic genes with low affinities (5). Recently, it was reported that p53 levels can vary in a series of discrete pulses; in this digital mode, the number of p53 pulses is positively related to the amount of DNA damage (6). Much work has explored the feedback mechanism of p53 oscillations (7–10). The p53-Mdm2 negative feedback loop is recognized as the basis of p53 oscillation (7), and additional positive feedback loops may make p53 oscillations more robust (8). On the contrary, it was suggested that the p53-PTEN (phosphatase and tensin homolog)-Akt-Mdm2 positive feedback loop may terminate oscillations by disrupting the p53-Mdm2 loop (9). Most recently, Batchelor et al. have shown that the ATM (ataxia telangiectasia mutated)-p53-Wip1 (wild-type p53-induced phosphatase 1) negative feedback loop is required for the generation of uniform p53 pulses (10). Therefore, it is important to further clarify how p53 pulses are initiated. Moreover, it is worth noting that p53 pulses were typically observed in MCF-7 human breast cancer cells (6), in which the *PTEN* gene cannot be expressed because of its promoter methylation (11). By contrast, *PTEN* can be transactivated by p53 in several cell lines including MCF-10A nontumorigenic mammary epithelial cells (12, 13). This raises the issue of whether p53 pulses can persist throughout the response in normal cells such as MCF-10A cells, because PTEN is induced late in the cellular response (12) and the p53-PTEN-Akt-Mdm2 loop may terminate p53 oscillations (9).

The physiological functions of p53 pulses have recently been explored (8, 14). It was suggested that the cell fate between survival and death may be determined by counting the number of p53 pulses. The strength of DNA damage is repeatedly evaluated; the cell survives after transient p53 pulses, or apoptosis is induced by sustained p53 pulses. This may represent a reliable and flexible mechanism; for example, it can avoid the premature apoptosis resulting from large accidental fluctuations in p53 levels (15). Nevertheless, it may take several hours to initiate apoptosis by p53 pulses even after a decision is taken favoring the death (14). By comparison, high constant levels of p53 may trigger apoptosis quickly once a choice is made in irreparably damaged cells. Therefore, it is tempting to explore whether both the analog and digital modes of p53 activation are exploited in one cellular response.

Motivated by the above considerations, we developed a four-module model to examine the connection between the dynamics of the p53 network and the DNA damage response. The model can depict the whole process from the generation and repair of DNA damage to the determination of cell fate between life and death. For repairable DNA damage, there is only one phase in p53 dynamics: A few pulses are produced before the damage is fixed. For irreparable DNA damage, there exist two phases: The concentration of p53 first shows a series of pulses and then switches to high constant levels, and apoptosis ensues. Thus, the analog and digital response modes are combined to guarantee a reliable decision and quick induction of apoptosis. We also stressed that the ATM-p53-Wip1 loop is essential for the generation of p53 pulses and that the level of PTEN determines whether p53 acts as a pulse generator or a switch in the second phase. Our results are in good agreement with experimental observations and may provide clues to p53-based cancer treatment.

Author contributions: X.-P.Z., F.L., and W.W. designed research, performed research, analyzed data, and wrote the paper.

The authors declare no conflict of interest.

*This Direct Submission article had a prearranged editor.

Freely available online through the PNAS open access option.

[1]To whom correspondence may be addressed. E-mail: fliu@nju.edu.cn or wangwei@nju.edu.cn.

This article contains supporting information online at www.pnas.org/lookup/suppl/doi:10.1073/pnas.1100600108/-/DCSupplemental.

Model and Methods

The response of the p53 network to DNA damage can be envisioned as a signal transduction process (16). We constructed an integrative model of the p53 network composed of four modules: a DNA repair module, an ATM sensor, a p53-centered feedback control module, and a cell fate decision module (Fig. 1). Three important feedback loops are included, namely the p53-Mdm2, ATM-p53-Wip1, and p53-PTEN-Akt-Mdm2 loops, which have been suggested to regulate p53 activity significantly (7, 9, 10).

Our model is able to characterize the process from the generation and repair of DNA damage to the choice of cell fate. Upon ionizing radiation (IR), double-strand breaks (DSBs) are produced and DNA repair proteins are quickly recruited to break sites, forming DSB–protein complexes (DSBCs) (17). For a population of cells exposed to the same radiation dose of D_{IR}, the initial numbers of DSBs are assumed to obey a Poisson distribution with a mean of $35 \times D_{IR}$ (18). Because repair proteins are much fewer than DSBs in most cases (7), we assume that there are 20 repair proteins per cell. ATM is activated by DNA damage through auto-phosphorylation, transiting from inactive dimer (ATM_2) to phosphorylated monomer (ATM^*) (19). Subsequently, p53 is stabilized and activated by phosphorylation (20), converting from inactive p53 to active $p53^*$. Active p53 induces expression of Mdm2, which in turn targets p53 for degradation, enclosing a negative feedback loop (2). Only nuclear p53 is considered here, whereas three forms of Mdm2 are included, namely $Mdm2_c$ (unphosphorylated cytoplasmic form), $Mdm2_{cp}$ (phosphorylated cytoplasmic form), and $Mdm2_n$ (nuclear form).

Based on its different phosphorylation status, active p53 can be further distinguished between p53 arrester and p53 killer, separately inducing cell cycle arrest and apoptosis (21). For simplicity, here p53 arrester refers to p53 primarily phosphorylated at Ser-15 and Ser-20, whereas p53 killer is p53 further phosphorylated at Ser-46. It is assumed that p53 arrester transactivates *p21*, *Wip1*, and *p53DINP1* (p53-dependent damage inducible nuclear protein 1), whereas p53 killer transactivates *p53DINP1*, *p53AIP1* (p53-regulated apoptosis-inducing protein 1), and *PTEN* (12, 21–24). The conversion between p53 arrester and p53 killer is controlled by Wip1 and p53DINP1 (22, 23). As a phosphatase, Wip1 promotes the dephosphorylation of ATM^* (25). Thus, there exists a negative feedback between ATM and p53 arrester via Wip1. Phosphorylated Akt (Akt^*) promotes the nuclear translocation of Mdm2 by phosphorylating $Mdm2_c$ (26). The phosphorylation of Akt is phosphatidylinositol 3,4,5-trisphosphate (PIP3)-dependent (27). On the other hand, PTEN promotes the transition from PIP3 to PIP2 (phosphatidylinositol 4,5-biphosphate) (28). Thus, there exists a double-negative feedback loop involving p53 killer, PTEN, Akt, and Mdm2.

The downstream targets of p53 directly control cellular outcomes. Among them, p21 induces cell cycle arrest, whereas p53AIP1 promotes apoptosis by inducing the release of mitochondrial cytochrome *c* (CytoC) into the cytoplasm (21). Released CytoC then activates caspase 3 (Casp3), and apoptosis ensues. A positive feedback between CytoC release and Casp3 activation is considered here (29). This feedback loop is crucial for the irreversible apoptosis induction, and similar irreversibility owning to positive feedback loops is exploited in stem cell differentiation (30). For simplicity, we did not model the formation of apoptosomes and activation of caspase 9 (31); rather, the persistent activation of Casp3 is considered the marker of apoptosis here.

The model implementation details are presented in *SI Appendix*. The process of DNA repair was simulated by the Monte Carlo method based on the two-lesion kinetic model (7, 32) (see *SI Appendix, Supplemental Method S1*). The dynamics of proteins in the other modules are characterized by ordinary differential equations (see *SI Appendix, Supplemental Method S2*). Eqs. **S1–S19** characterize the dynamics of three p53-centered feedback loops, and Eqs. **S20–S23** characterize the dynamics of p21, p53AIP1, CytoC, and Casp3. Specifically, the ATM-dependent activation of p53 and Mdm2-mediated degradation of p53 (Eqs. **S5–S7**), together with the conversion between p53 arrester and p53 killer mediated by Wip1 and p53DINP1 (Eqs. **S15** and **S16**), are key steps in regulating p53 activity. The definition of each variable and parameter values are listed in Tables S1 and S2, respectively. The bifurcation diagrams were plotted by using the free softwares XPPAUT and Oscill8. The units of time and radiation dose are minute and Gy, respectively, and the units of other parameters ensure that the concentrations of proteins are dimensionless.

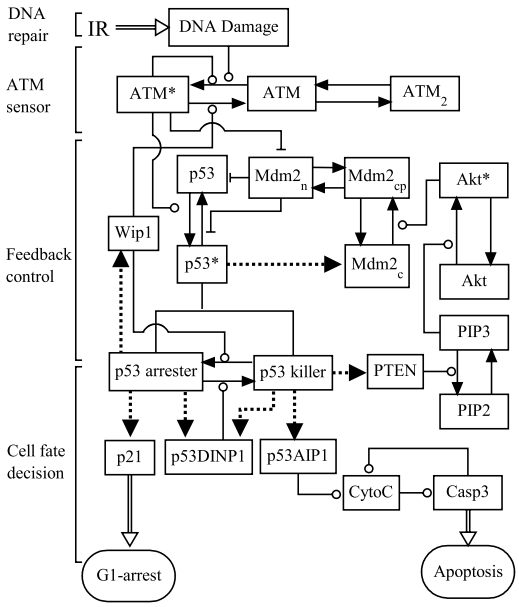

Fig. 1. Schematic depiction of the integrative model. The model is composed of four modules, separately characterizing the DNA repair, ATM sensor, p53-centered feedback control, and cell fate decision. Four feedback loops are considered, i.e., the p53-Mdm2 and the p53-Wip1-ATM negative feedback loop, and the p53-PTEN-Akt-Mdm2 and the CytoC-Casp3 positive feedback loop. The transactivation of target genes by p53 is denoted by dotted lines. State transition is represented by arrow-headed solid lines, and the promotion and inhibition of state transition are separately denoted by circle-headed and bar-headed lines. Other processes are depicted by arrow-headed double lines.

Results

Overview of the Dynamics of the p53 Network. We first present an overview of the network dynamics by displaying the output of each module at two typical radiation doses in Fig. 2. The number of DSBCs, n_c, indicates the presence of DNA damage. n_c quickly rises to its maximum (i.e., the number of repair proteins per cell) upon DNA damage and stays there until the number of DSBs falls below 20.

At $D_{IR} = 3$ Gy, the concentrations of ATM^*, $p53^*$, and p21 undergo three pulses followed by basal levels, whereas Casp3 level remains low (Fig. 2*A*). Accordingly, the cell cycle is first arrested by p21, and the cell recovers to normal proliferation after DNA damage is fixed. At $D_{IR} = 5$ Gy, four pulses are first produced in ATM^*, $p53^*$, and p21 levels; then the concentrations of ATM^*, $p53^*$, and Casp3 quickly rise to high levels (at different rates), whereas p21 returns to basal levels (Fig. 2*B*). In this case, the cell undergoes apoptosis. Thus, the cellular response to irreparable DNA damage is divided into two phases. In the first phase, the cell cycle arrest allows time to fix DNA damage, and the cell repeatedly checks for the presence of DSBs via oscillations in protein levels. This provides a robust mechanism for committing the cell to apoptosis, avoiding unnecessary death (15). If the damage is not fixed after four pulses, the apoptotic decision

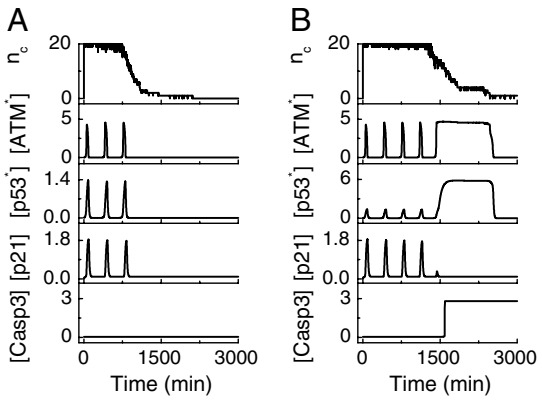

Fig. 2. Overview of the dynamics of the p53 network. Time courses of n_c and the levels of ATM*, p53*, p21, and Casp3 at $D_{IR} = 3$ Gy (*A*) or 5 Gy (*B*).

is taken, and the caspase cascade is quickly initiated in the second phase.

Therefore, depending on the amount of DNA damage, the network may exhibit the one- or two-phase dynamics; the first and the second phase are characterized by pulsatile and switch-like behaviors of p53, respectively. As a result, a reliable choice is made between life and death, and apoptosis is quickly induced once necessary. Such a two-phase mode of p53 response may represent an optimal mechanism, having advantages over the purely analog or digital control mode mentioned above.

Recurrent Initiation of p53 Pulses by ATM Pulses. It is worthy to clarify the contributions of different feedback loops to the generation of p53 pulses. Here, we mainly investigated the effects of two negative feedback loops, namely the p53-Mdm2 and the ATM-p53-Wip1 loop (because PTEN is induced during the late phase (12), we can ignore the positive feedback loop involving PTEN in this section). It is important to determine whether both the loops are indispensable for p53 pulses.

Fig. 3*A* shows the bifurcation diagram of ATM* level versus n_c. ATM* level remains low for small n_c, and a Hopf bifurcation appears near $n_c = 7$, beyond which ATM* level can undergo repeated oscillations with nearly the same amplitude over a wide range of n_c. That is, such minor DNA damage as caused by the IR of 0.2 Gy can be sensed by ATM (19); thus, ATM acts as a sensitive and reliable detector of IR-induced DNA damage.

The ATM oscillations depend remarkably on Wip1, which is regulated mainly by p53. We plotted the bifurcation diagram of ATM* level versus the p53-inducible synthesis rate of Wip1, k_{swip1}, to characterize the effect of Wip1 on the generation of ATM oscillations (Fig. 3*B*). For $k_{swip1} < 0.0585$, ATM* level settles in a higher steady state (the other two steady states are unstable). When $k_{swip1} \geq 0.0585$, ATM* level can undergo oscillations, and the amplitude drops with increasing k_{swip1}. Thus, a sufficient amount of Wip1 is required for ATM oscillations, whereas excessive Wip1 tends to reduce the amplitude of oscillation. Our results are consistent with the experimental observations that removal of Wip1 leads to high levels of phosphorylated ATM and that overexpression of Wip1 leads to reduction in ATM phosphorylation (10).

The ATM-p53-Wip1 loop with an intrinsic time delay is important for the generation of p53 pulses. Over one period, ATM* level first rises, and p53 then gradually accumulates to a peak level, accompanied by an increase in Wip1 level (Fig. 3*C*). Wip1 then inhibits ATM* activity, and its level drops quickly. After a delay, p53* level also falls, while Wip1 level decreases at a slower rate. Note that ATM can be reactivated by residual DNA damage, and p53 is subsequently activated again. Thus, p53 pulses are recurrently driven by ATM pulses, which is in agreement with the experimental findings (10). Moreover, owing

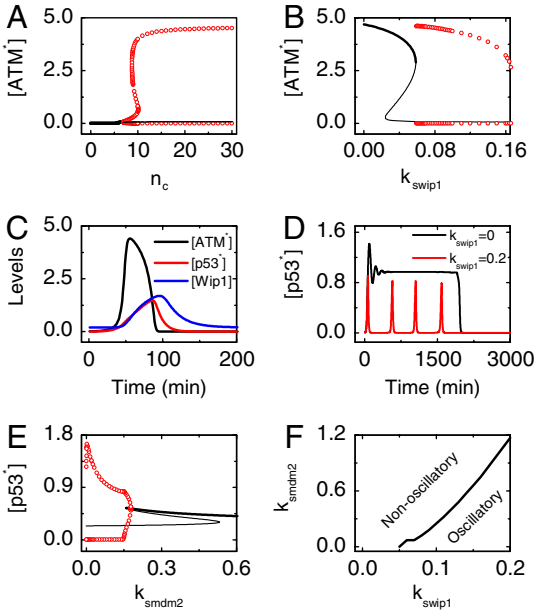

Fig. 3. Initiation of p53 pulses by ATM pulses. (*A–B*) The bifurcation diagram of ATM* level vs. n_c (*A*) and that of ATM* level vs. k_{swip1} (*B*) with $n_c = 20$. The stable and unstable steady states are indicated by thick and thin black lines, respectively. The minima and maxima of the limit cycles are denoted by open circles. (*C*) A single pulse in the levels of p53*, ATM*, and Wip1 at $D_{IR} = 1$ Gy. (*D*) Time course of p53* level with $k_{swip1} = 0$ or 0.2 at $D_{IR} = 4$ Gy. (*E*) The bifurcation diagram of p53* level vs. k_{smdm2} with $n_c = 20$. The same convention is used as in panels *A* and *B*. (*F*) The parameter plane spanned by k_{swip1} and k_{smdm2} is divided into two regions, separately corresponding to oscillatory and nonoscillatory behaviors of p53.

to stochasticity in the generation and repair of DNA damage, there exists considerable variability in the responses of individual cells to the same IR, as seen in the time courses of ATM* and Wip1 levels for three cells at $D_{IR} = 5$ Gy (Fig. S1).

Fig. 3*D* displays the temporal evolution of p53* level with different k_{swip1}. For $k_{swip1} = 0$, that is, the ATM-p53-Wip1 loop is shut off, the concentration of p53* converges to a constant level during the repair of DNA damage. For $k_{swip1} = 0.2$, however, four pulses are still generated although the amplitude becomes lower. Therefore, the ATM-p53-Wip1 loop is necessary for the generation of p53 pulses.

We further examined the role of the p53-Mdm2 loop in the generation of p53 pulses, focusing on the influence of the p53-inducible synthesis rate of Mdm2, k_{smdm2}. In the bifurcation diagram (Fig. 3*E*), p53* level stays in an upper steady state (the middle and lower steady states are unstable) for $k_{smdm2} \geq 0.178$. Only when $k_{smdm2} < 0.178$ can pulses be evoked, and the amplitude drops with increasing k_{smdm2} over a wide range. Notably, the presence of p53 oscillations at $k_{smdm2} = 0$ indicates that disrupting the p53-Mdm2 loop does not terminate p53 oscillation. The temporal evolution of p53* level with different k_{smdm2} is consistent with Fig. 3*E* (Fig. S2*A*). Whereas the concentration of p53* slowly converges to a constant level in a damped-oscillation manner at $k_{smdm2} = 0.2$, four p53 pulses are induced at $k_{smdm2} = 0$. This implies that the p53-Mdm2 loop becomes redundant for p53 oscillations when the ATM-p53-Wip1 loop is present. We also assessed the role of the p53-Mdm2 loop in the induction of p53 pulses in the model proposed by Batchelor et al. (10), where an explicit time delay was introduced (Fig. S2*B*). Similarly, there appear several p53 pulses in the absence of p53-induced *Mdm2* expression. Therefore, the p53-Mdm2 loop may be dispensable for the generation of p53 pulses in the presence of another negative feedback loop.

On the k_{swip1}-k_{smdm2} parameter plane, the p53 dynamics are divided into oscillatory and nonoscillatory regimes (Fig. 3*F*). To generate p53 oscillations, the ATM-p53-Wip1 loop must be present with $k_{swip1} > 0.0585$; the area of oscillation region almost linearly enlarges with increasing k_{swip1}. By contrast, enhancing the expression of Mdm2 shrinks the oscillation region. Taken together, these results suggest that the ATM-p53-Wip1 loop is essential for the generation of p53 pulses, whereas the p53-Mdm2 loop may have a role in fine tuning the shape of p53 pulses.

Two-Phase Dynamics of the Network. Here, we reveal the dynamics of several proteins in the p53 network. Fig. 4*A* displays the temporal evolution of p53*, $Mdm2_n$, $Mdm2_c$, Akt* and PTEN levels at $D_{IR} = 3$ Gy. Three p53 pulses are triggered during the repair of DNA damage. The intervals between successive pulses are about 6 hr, and the amplitudes are almost invariable, consistent with the experimental observations of digital p53 pulses (6). Because PTEN is expressed only at basal levels, most of Mdm2 is phosphorylated by active Akt and enters the nucleus. Thus, only a small amount of Mdm2 remains in the cytoplasm. After the cell recovers to normal proliferation, p53* returns to basal levels, whereas Akt* level remains constant and $Mdm2_n$ level is significantly larger than zero.

At $D_{IR} = 5$ Gy, the dynamics of the proteins undergo two phases (Fig. 4*B*). In the first phase, four pulses are produced in p53* and $Mdm2_n$ levels, while active Akt stays at constant levels without PTEN induction. During the second phase, Akt is deactivated by PTEN, which accumulates and reaches a constant level. Thus, the concentration of p53* switches to a rather high level because the nuclear entry of Mdm2 is blocked. Notably, p53 and Akt counteract each other. Our results are also consistent with the findings that PTEN becomes remarkable only during the late phase of the cellular response to IR (12). The two-phase p53 dynamics result from two aspects of regulation: The loss of Wip1 induction relieves its inhibitory effect on ATM, elevating p53 level, and the full activation of p53 by PTEN further drives p53 to rather high levels by sequestering Mdm2 in the cytoplasm. Such a two-phase dynamical behavior of the p53 network awaits experimental identification.

Dynamics and Functions of p53 Arrester and p53 Killer. We further investigated the dynamics of p53 arrester and p53 killer, which are directly associated with the ultimate cell fate. At $D_{IR} = 3$ Gy, only pulses of p53 arrester and its downstream targets are triggered (Fig. S3*A*). At $D_{IR} = 5$ Gy, p53 arrester shows four pulses in the first phase and then remains at basal levels, whereas the concentration of p53 killer switches from basal levels to high levels in the second phase (Fig. 5*A* and Fig. S3*B*). Thus, p53 arrester and p53 killer predominate in the first and the second phase, respectively. The p53 arrester transactivates Wip1, p53DINP1, and p21, which induces cell cycle arrest in the first phase. The p53 killer induces PTEN, p53DINP1, and p53AIP1, which are proapoptotic, and thus apoptosis will be initiated in the second phase (Fig. 5*B*). The transition between p53 arrester and p53 killer is controlled by Wip1 and p53DINP1; the conversion occurs when the temporal integration of p53DINP1 reaches a certain threshold. Moreover, because the stochasticity in the generation and repair of DNA damage is transmitted to downstream modules, the dynamics of two forms of active p53 and their downstream targets are also variable from cell to cell (Fig. S4).

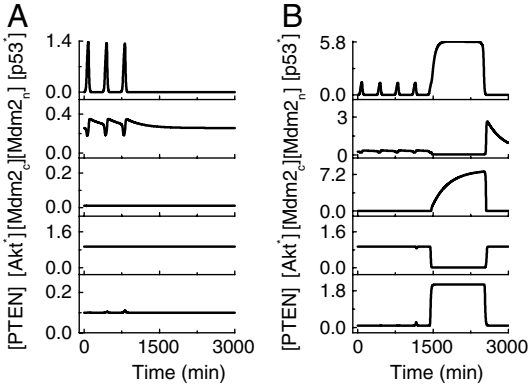

Fig. 4. Temporal evolution of the levels of proteins in the p53-centered feedback loops at $D_{IR} = 3$ Gy (*A*) or 5 Gy (*B*).

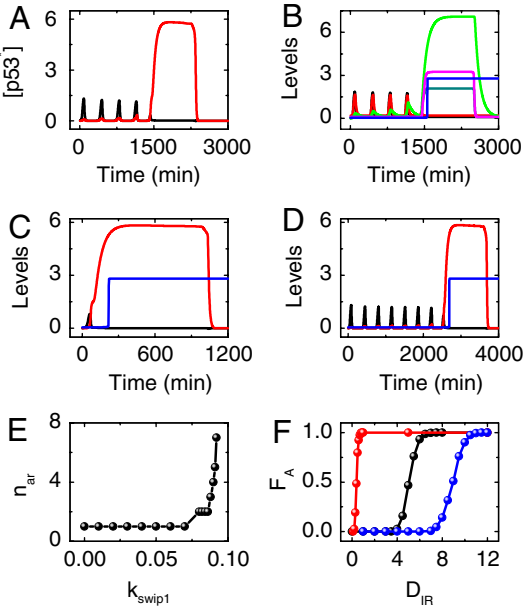

Fig. 5. Dynamics of two forms of active p53 and their downstream targets. (*A*) Time courses of the levels of p53 arrester (black) and p53 killer (red) at $D_{IR} = 5$ Gy. (*B*) Temporal evolution of the levels of p21 (black), Wip1 (red), p53DINP1(green), PTEN (cyan), p53AIP1 (purple), and Casp3 (blue) at $D_{IR} = 5$ Gy. (*C–D*) Time courses of the concentrations of p53 arrester (black), p53 killer (red), and Casp3 (blue) with $k_{swip1} = 0$ and $D_{IR} = 1$ Gy (*C*) or $k_{swip1} = 0.092$ and $D_{IR} = 10$ Gy (*D*). (*E*) The number of pulses in p53 arrester preceding apoptosis induction, n_{ar}, as a function of k_{swip1}. (*F*) The fraction of apoptotic cells in a population of 2,000 cells, F_A, vs. D_{IR} with $k_{swip1} = 0$ (red), 0.09 (black), or 0.092 (blue).

In the following, we systematically explored how Wip1 affects the radiosensitivity of cells via modulating the conversion between p53 arrester and p53 killer. Without p53-inducible synthesis of Wip1 ($k_{swip1} = 0$), p53 killer is induced quickly after one pulse of p53 arrester, and apoptosis is triggered soon even at $D_{IR} = 1$ Gy (Fig. 5*C*). That is, Wip1-deficient cells become ultrasensitive to irradiation. This is consistent with the role of Wip1 as an oncogenic regulator in stress-induced apoptosis (33). By contrast, in Wip1-proficient cells it takes a long time for p53 killer to predominate over p53 arrester even at $D_{IR} = 10$ Gy (Fig. 5*D*). Thus, the induction of apoptosis is significantly postponed, and the cell becomes resistant to irradiation when Wip1 is overexpressed. This may partially explain how Wip1 acts as an oncogene and why it is frequently overexpressed in several cancers (33). The marked influence of Wip1 levels on the radiosensitivity of cells results form its role in preventing the primary activation of p53 via ATM and further activation by attenuating its phosphorylation at Ser-46 (22).

We also examined how the number of pulses in p53 arrester required for apoptosis induction, n_{ar}, varies with k_{swip1}. When $k_{swip1} < 0.07$, apoptosis is triggered after a single pulse of p53 arrester at $D_{IR} = 1$ Gy (Fig. 5*E*). But n_{ar} rises remarkably when $k_{swip1} \geq 0.07$. That is, high levels of Wip1 slow down the convention from p53 arrester to p53 killer. Thus, the transition between p53 arrester and p53 killer is significantly influenced by the level

of Wip1. Moreover, the effects of other parameters involved in the ATM-p53-Wip1 loop on the robustness of the two-phase dynamics of p53 are characterized in Table S3.

As reported above, the responses of individual cells exhibit remarkable variability even when they are exposed to the same IR. The fraction of apoptotic cells, F_A, versus D_{IR} was plotted to exhibit the effect of Wip1 on cell fate decision at the population level (Fig. 5*F*). The curves look like a sigmoidal function. In the normal case, apoptosis first appears at $D_{IR} = 4$ Gy, and all cells die at $D_{IR} = 7.5$ Gy. In the Wip-deficient case, the curve shifts leftward, and apoptosis first appears at $D_{IR} = 0.2$ Gy and all cells die at $D_{IR} = 0.9$ Gy. When Wip1 is overexpressed, however, the curve shifts rightward, and apoptosis first appears at $D_{IR} = 7$ Gy. That is, cells become resistant to stress signals. Taken together, Wip1 has a marked effect on cell fates and may be an important target of cancer therapy.

The Role of PTEN in p53-Mediated Cell Fate Decision. We have demonstrated that Wip1 has a key role in generating p53 pulses during the first phase, whereas PTEN contributes to full activation of p53 in the second phase. The effect of PTEN on p53 activity and cell fate decision is further characterized in detail in this section.

Fig. 6*A* displays the bifurcation diagram of p53* level versus the p53-inducible synthesis rate of PTEN, k_{sPTEN}. For $k_{sPTEN} < 0.093$, p53* remains in a low steady state. When $0.093 \le k_{sPTEN} < 0.119$, oscillations can be evoked in p53* level. For $0.119 \le k_{sPTEN} < 0.155$, p53* level settles in an upper steady state (the other two steady states are unstable). When $k_{sPTEN} \ge 0.155$, p53* remains at high levels. Thus, PTEN significantly affects the dynamics of p53 in the second phase. Moreover, the influences of other parameters involved in the p53-PTEN-Akt-Mdm2 loop on the robustness of p53 dynamics are further analyzed in Table S3.

Considering that p53 killer is the dominant form of p53* in the second phase and its level is close to p53* level, here we investigated only the temporal evolution of p53 killer with different k_{sPTEN}. Clearly, p53 killer converges to a lower level after damped oscillations at $k_{sPTEN} = 0$, and Casp3 cannot be activated (Fig. 6*B*). For an intermediate value of k_{sPTEN}, p53 killer shows a series of pulses, and Casp3 is activated to trigger apoptosis. As expected, p53 killer quickly rises to a high level at $k_{sPTEN} = 0.2$, and Casp3 is activated fast. Note that PTEN affects the network dynamics by modulating the relative predominance of the p53-PTEN-Akt-Mdm2 loop over the p53-Mdm2 loop because it inhibits the nuclear translocation of Mdm2 (26). Only when the strength of these two loops becomes comparable, they cooperate to trigger p53 pulses (34). In the other cases, p53 remains at low or rather high levels, depending on which loop predominates.

We also explored the effect of PTEN on apoptosis induction at the cell population level (Fig. 6*C*). Apoptosis first appears at $k_{sPTEN} = 0.1$, and the fraction of apoptotic cells, F_A, gets saturated when $k_{sPTEN} > 0.2$. Moreover, there exists only a slight difference in F_A between the cases separately with $k_{sPTEN} = 0.105$ and 0.2 (Fig. 6*C*, *Inset*). We further investigated the influence of PTEN on the timing of apoptosis induction (Fig. 6*D*). Almost all apoptosis is initiated around 1,520 min for $k_{sPTEN} = 0.2$ (the irradiation is applied at time 0). For $k_{sPTEN} = 0.105$, besides the main peak around 1,600 min, two other peaks separately appear near 1,900 and 2,150 min, indicating that apoptosis is induced after two or three pulses of p53 killer. In this case, about 60% of the apoptosis happens after one pulse of p53 killer. Thus, there exists more variability in apoptosis induction mediated by pulses of p53 killer, whereas quick induction of apoptosis evoked by high levels of p53 remarkably reduces the response heterogeneity. Taken together, PTEN is important for killing irreparably damaged cells and may act as another target of cancer therapy.

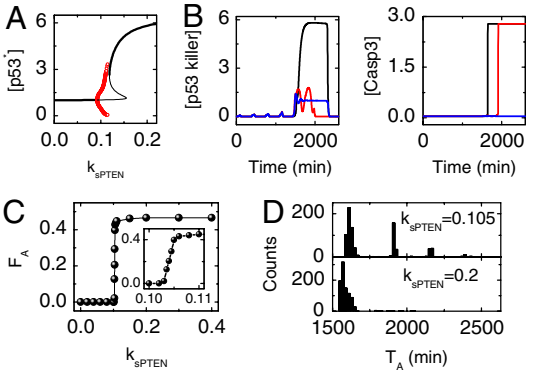

Fig. 6. Effect of PTEN on p53 dynamics and cell fate decision. (*A*) The bifurcation diagram of p53* level vs. k_{sPTEN} with $n_c = 20$. The stable and unstable steady states are indicated by thick and thin black lines, respectively. The minima and maxima of the limit cycles are denoted by open circles. (*B*) Time courses of the levels of p53 killer and Casp3 with $k_{sPTEN} = 0$ (blue), 0.105 (red), or 0.2 (black). (*C*) The fraction of apoptotic cells in a population of 2,000 cells vs. k_{sPTEN} at $D_{IR} = 5$ Gy. The inset is a zoom in of the curve. (*D*) The histograms of timing of apoptosis induction, T_A (defined as the time point of Casp3 activation), with $k_{sPTEN} = 0.015$ or 0.2. The time bin is 20 min.

Discussion

The p53-Mediated DNA Damage Response. In this work, we constructed an integrative model of the p53 network to clarify the link between p53 dynamics and the DNA damage response. Our results support the notion that p53 is activated in a progressive manner. First, p53 is primarily modified (such as phosphorylation at Ser-15 and Ser-20) and accumulates in pulses to induce protective cell cycle arrest for repairable DNA damage; it is further modified (such as phosphorylation at Ser-46) and fully activated to induce apoptosis for irreparable DNA damage (35). The pulsing behavior of p53 in the first phase exerts a reliable and flexible control, avoiding the premature apoptosis. The high plateau levels of p53 in the second phase guarantee the quick induction of apoptosis after the apoptotic decision is taken. These results clearly demonstrate that both the levels and posttranslational modifications of p53 regulate the cellular response to DNA damage. Moreover, the sequential induction of Wip1 and PTEN by p53 in turn modulates p53 activity by changing the predominance of distinct feedback loops during the response.

Oscillation and Bistability in p53 Dynamics. There has been much theoretical work on the mechanism of p53 oscillation (7, 8, 14). Moreover, p53 dynamics may also exhibit bistability (36). However, most models ignored the possible association between the oscillatory and bistable behaviors of p53. Puszynski et al. first combined oscillation and bistability in their model (9). Nevertheless, they only considered the p53-Mdm2 loop, which alone can trigger only continuous p53 oscillations rather than discrete p53 pulses as observed experimentally (6). Moreover, the mechanism for apoptosis induction is not robust enough because the higher steady-state levels of p53 are comparable to the peaks of p53 oscillations. In our model, however, the p53 pulses are triggered by ATM pulses, well consistent with experimental observations (10), and rather high levels of p53 are maintained to induce apoptosis. Constrained by experimental data, we ignored intrinsic noise from gene expression, which may be important under some conditions. For example, the intrinsic noise resulting from extinction and resurrection of proteins can induce bistability in the deterministically monostable system (37). In our work, fluctuations in the levels of Wip1 and PTEN owing to intrinsic noise may make p53 dynamics more variable among cells. Thus, it is intriguing to further investigate the effect of intrinsic noise on cell fate decision.

An Optimal Mode of p53 Response to DNA Damage. It is worth comparing the present work with the previous one on p53 dynamics

(14), in which p53 responds to DNA damage only in a series of pulses. The cell fate decision is governed by the number of p53 pulses, which may represent a robust mechanism. But when triggered by proapoptotic p53 pulses, it may take several hours to initiate apoptosis after the decision; this is inefficient in killing irreparable cells. In the present work including the ATM-p53-Wip1 and p53-PTEN-Akt-Mdm2 loops, the two-phase dynamics of p53 occur in irreparably damaged cells. The pulses of p53 induce cell cycle arrest and ensure a reliable choice, whereas high constant levels of p53 promote the quick execution of apoptosis. That is, the advantage of p53 pulses as a molecular timer for decision-making is retained, whereas the deficiency with p53 pulses in apoptosis induction is overcome in the current work. We also demonstrated how Wip1 and PTEN can remarkably regulate p53 dynamics. Moreover, the underlying connection between p53 dynamics and cellular outcomes is clearly clarified. In sum, the two-phase mode of p53 response may represent an optimal mechanism, taking advantage of the benefits of both the digital and analog modes.

Plausibility of the Two-Phase Dynamics of p53. The two-phase dynamics of the p53 network are compatible with experimental observations. It was reported that Wip1 and PTEN are induced by p53 during the early and late phases of the cellular response, respectively (12, 24). Thus, the ATM-p53-Wip1 loop may cooperate with the p53-Mdm2 loop to elicit p53 pulses in the early phase, whereas the p53-PTEN-Akt-Mdm2 loop may become dominant later and drive p53 to high levels (Fig. S5). Our results are consistent with the finding that it is p21 rather than the proapoptotic proteins that undergoes pulses in the DNA damage response (10). Moreover, it is worthy to note that typical p53 pulses were experimentally observed in the transformed MCF-7 cells, in which *PTEN* cannot be expressed because of methylation in its promoter (11). It is expected to validate the two-phase dynamics of p53 in MCF-10A cells, in which the above three feedback loops are all intact, or by transfecting MCF-7 cells with *PTEN* under the control of p53-responsive promoter. Furthermore, it is promising to explore the multiple-phase dynamics in other systems like the sporulation-competence decision system, in which there exist three stages in the decision-making process (38).

Implications of p53 Dynamics in Cancer Treatment. The two-phase model of p53 activity may provide clues to cancer treatment. Our results suggest that p53 pulses play a prosurvival role by inducing cell cycle arrest and facilitating DNA repair. We propose that sustained p53 pulses may extensively exist in cancer cells with proficient Wip1. Thus, RNA inference may be exploited to reduce Wip1 expression in those cells so that they can be killed quickly by shortening the protective cell cycle arrest. On the other hand, PTEN contributes to apoptosis induction by fully activating p53. Thus, reactivation of PTEN in some cancer cells may greatly enhance the p53-dependent apoptosis and improve the treatment efficiency. Therefore, our work suggests that regulation of p53 dynamics may be an efficient way to improve the therapy efficacy.

ACKNOWLEDGMENTS. This work was supported by the National Basic Research Program of China (2007CB814806), the National Natural Science Foundation of China (10834002), the Natural Science Foundation of Jiangsu Province (BK2009008), and the Program for New Century Excellent Talents in Universities (NCET-08-0269).

1. Murray-Zmijewski F, Slee EA, Lu X (2008) A complex barcode underlies the heterogeneous response of p53 to stress. *Nat Rev Mol Cell Biol* 9:702–712.
2. Wu X, Bayle JH, Olson D, Levine AJ (1993) The p53-mdm2 autoregulatory feedback loop. *Genes Dev* 7:1126–1132.
3. Aylon Y, Oren M (2007) Living with p53, dying of p53. *Cell* 130:597–600.
4. Vousden KH, Lane DP (2007) p53 in health and disease. *Nat Rev Mol Cell Biol* 8:275–283.
5. Weinberg RL, Veprintsev DB, Bycroft M, Fersht AR (2005) Comparative binding of p53 to its promoter and DNA recognition elements. *J Mol Biol* 348:589–596.
6. Lahav G, et al. (2004) Dynamics of the p53-Mdm2 feedback loop in individual cells. *Nat Genet* 36:147–150.
7. Ma L, et al. (2005) A plausible model for the digital response of p53 to DNA damage. *Proc Natl Acad Sci USA* 102:14266–14271.
8. Zhang T, Brazhnik P, Tyson JJ (2007) Exploring mechanisms of the DNA-damage response—p53 pulses and their possible relevance to apoptosis. *Cell Cycle* 6:85–94.
9. Puszynski K, Hat B, Lipniacki T (2008) Oscillations and bistability in the stochastic model of p53 regulation. *J Theor Biol* 254:452–465.
10. Batchelor E, et al. (2008) Recurrent initiation: a mechanism for triggering p53 pulses in response to DNA damage. *Mol Cell* 30:277–289.
11. Garcia JM, et al. (2004) Promoter methylation of the PTEN gene is a common molecular change in breast cancer. *Genes Chromosome Cancer* 41:117–124.
12. Stambolic V, et al. (2001) Regulation of PTEN transcription by p53. *Mol Cell* 8:317–325.
13. Burnett GT, Weathersby DC, Taylor TE, Bremner TA (2008) Regulation of inflammation- and angiogenesis-related gene expression in breast cancer cells and co-cultured macrophages. *Anticancer Res* 28:2093–2099.
14. Zhang X-P, Liu F, Cheng Z, Wang W (2009) Cell fate decision mediated by p53 pulses. *Proc Natl Acad Sci USA* 106:12245–12250.
15. Lahav G (2004) The strength of indecisiveness: Oscillatory behavior for better cell fate determination. *Sci STKE* 2004:pe55.
16. Batchelor E, Loewer A, Lahav G (2009) The ups and downs of p53: Understanding protein dynamics in single cells. *Nat Rev Cancer* 9:371–377.
17. Rothkamm K, Kruger I, Thompson LH, Lobrich M (2003) Pathways of DNA double-strand break repair during the mammalian cell cycle. *Mol Cell Biol* 23:5706–5715.
18. Rothkamm K, Lobrich M (2003) Evidence for a lack of DNA double-strand break repair in human cells exposed to very low X-ray doses. *Proc Natl Acad Sci USA* 100:5057–5062.
19. Bakkenist CJ, Kastan MB (2003) DNA damage activates ATM through intermolecular autophosphorylation and dimer dissociation. *Nature* 421:499–506.
20. Prives C (1998) Signaling to p53: Breaking the MDM2-p53 circuit. *Cell* 95:5–8.
21. Oda K, et al. (2000) p53AIP1, a potential mediator of p53-dependent apoptosis, and its regulation by Ser-46-phosphorylated p53. *Cell* 102:849–862.
22. Takekawa M, et al. (2000) p53-inducible Wip1 phosphatase mediates a negative feedback regulation of p38 MAPK-p53 signaling in response to UV radiation. *EMBO J* 19:6517–6526.
23. Okamura S, et al. (2001) p53DINP1, a p53-inducible gene, regulates p53-dependent apoptosis. *Mol Cell* 8:85–94.
24. Mayo LD, et al. (2005) Phosphorylation of human p53 at Serine 46 determines promoter selection and whether apoptosis is attenuated or amplified. *J Biol Chem* 280:25953–25959.
25. Shreeram S, et al. (2006) Wip1 phosphatase modulates ATM-dependent signaling pathways. *Mol Cell* 23:757–764.
26. Mayo LD, Donner DB (2001) A phosphatidylinositol 3-kinase/Akt pathway promotes translocation of Mdm2 from the cytoplasm to the nucleus. *Proc Natl Acad Sci USA* 98:11598–11603.
27. Manning BD, Cantley LC (2007) AKT/PKB signaling: Navigating downstream. *Cell* 129:1261–1274.
28. Stambolic V, et al. (1998) Negative regulation of PKB/Akt-dependent cell survival by the tumor suppressor PTEN. *Cell* 95:29–39.
29. Kirsch DG, et al. (1999) Caspase-3-dependent cleavage of Bcl-2 promotes release of cytochrome c. *J Biol Chem* 274:21155–21161.
30. Wang J, Xu L, Wang EK, Huang S (2010) The potential landscape of genetic circuits imposes the arrow of time in stem cell differentiation. *Biophys J* 99:29–39.
31. Bao Q, Shi Y (2006) Apoptosome: A platform for the activation of initiator caspases. *Cell Death Differ* 14:56–65.
32. Stewart RD (2001) Two-lesion kinetic model of double-strand break rejoining and cell killing. *Radiat Res* 156:365–378.
33. Le Guezennec X, Bulavin DV (2010) WIP1 phosphatase at the crossroads of cancer and aging. *Trends Biochem Sci* 35:109–114.
34. Zhang X-P, Liu F, Wang W (2010) Coordination between cell cycle progression and cell fate decision by the p53 and E2F1 pathways in response to DNA damage. *J Biol Chem* 285:31571–31580.
35. Kruse J-P, Gu W (2009) Modes of p53 regulation. *Cell* 137:609–622.
36. Wee KB, Aguda BD (2006) Akt versus p53 in a network of oncogenes and tumor suppressor genes regulating cell survival and death. *Biophys J* 91:857–865.
37. Schultz D, Walczak AM, Onuchic JN, Wolynes PG (2008) Extinction and resurrection in gene networks. *Proc Natl Acad Sci USA* 105:19165–19170.
38. Schultz D, Wolynes PG, Jacob EB, Onuchic JN (2009) Deciding fate in adverse times: Sporulation and competence in Bacillus subtilis. *Proc Natl Acad Sci USA* 106:21027–21034.

Supporting Information (SI)

"Two-phase dynamics of p53 in the DNA damage response"

Xiao-Peng Zhang, Feng Liu, and Wei Wang

Supplemental Method S1: Model construction

The integrative model of the p53 network is composed of four modules, i.e., a DNA repair module, an ATM sensor module, a p53-centered feedback control module, and a cell fate decision module. The details of each module are presented as follows.

DNA repair module. The repair of DNA damage is characterized here. The typical form of DNA damage induced by ionizing radiation (IR) is DNA double-strand break (DSB) [1]. There are two pathways to repair DSBs: nonhomogeneous end-joining (NHEJ) and homologous repair (HR) [1]. HR is active only in S/G2 phases of the cell cycle since this pathway requires a sister chromatid as a template, while NHEJ simply associates two broken ends together [1]. Thus, NHEJ can function throughout the cell cycle and is the predominant repair pathway in mammalian cells, especially in the G1 phase. We refer to the NHEJ pathway in our model. It is noted that p53 has a role in DNA repair. But its effect on NHEJ is rather complicated and even controversial [2]; both stimulatory and inhibitory effects were reported [3–6]. For simplicity, here we did not consider the influence of p53 on DNA repair.

The repair of DSBs is typically considered as a biphasic process. Simple DSBs are repaired quickly, while complex DSBs are repaired rather slowly. The two-lesion kinetic (TLK) model has been developed to describe this biphasic repair process [7]. Based on the TLK model, we simulated the dynamics of DSB repair by the Monte Carlo method [8]. The detailed algorithm has been presented in the supplemental materials of our previous papers [9, 10], and the related parameters are listed in Supplemental Table S2. As in our previous studies, the initial numbers of DSBs within a cell population exposed to the radiation dose of $D_{\rm IR}$ are assumed to obey a Poisson distribution with an average of $35\times D_{\rm IR}$. This is consistent with the experimental measurements of 30∼40 DSBs per Gy per cell [11]. The number of repair proteins per cell is assumed to be 20 since they are usually limited compared to DSBs [8].

ATM sensor. ATM acts as a sensor of DSBs. In unstressed cells, ATM is inactive in dimers. Upon IR, the ATM dimer is disassociated into active monomer through intermolecular phosphorylation [12]. Thus, there exists a positive feedback loop in which ATM is activated by itself. Active ATM can activate p53. On the other hand, ATM can be inactivated by p53-inducible Wip1

through dephosphorylation, enclosing a negative feedback loop [13]. The dynamics of this module are characterized by Eqs. 1-3 in Supplemental Method S2, and the related parameters are listed in Supplemental Table S2.

The total level of ATM is assumed to be constant since it shows no remarkable variation after IR [12]. Three forms of ATM are considered, i.e., ATM_2 (inactive dimer), ATM (inactive monomer) and ATM^* (active monomer). Considering ATM dimers are predominant in unstressed case, we let $k_{\mathrm{dim}} \gg k_{\mathrm{undim}}$ in Eq. 1. The activation of ATM by DSBs is characterized by the n_c-dependent ATM activation rate, while the inhibition of ATM by Wip1 is represented in the deactivation rate of ATM (Eq. 2). Since the phosphorylation and dephosphorylation processes can be considered as enzyme-catalyzed reactions, they are assumed to follow the Michaelis-Menten kinetics [14].

p53-centered feedback control module. The p53-centered feedback loops play a key role in the activation and regulation of p53 activity. Active ATM activates p53 by two ways, phosphorylating p53 to disassociate it from Mdm2 and phosphorylating Mdm2 to degrade it [15, 16]. In the model, we consider two forms of nuclear p53, i.e., $p53^*$ (phosphorylated, active form) and p53 (unphosphorylated, inactive form). The function of cytoplasmic p53 is not involved in this model although it can play a transcription-independent role in apoptosis induction [17], and we have considered the effect of cytoplasmic p53 in another work [18]. Three forms of Mdm2 are considered, namely $Mdm2_n$ (nuclear form), $Mdm2_c$ (unphosphorylated cytoplasmic form), and $Mdm2_{cp}$ (phosphorylated cytoplasmic form). $p53^*$ induces the production of $Mdm2_c$, and $Mdm2_{cp}$ translocates to the nucleus, promoting the degradation of $p53^*$. This constitutes a negative feedback loop between p53 and Mdm2 [19].

The dynamics of this module are mainly described by Eqs. 4-14 in Supplemental Method S2. Considering the tetramer of p53 as a transcription factor [20], the p53-induced Mdm2 production is characterized by a Hill function, and the Hill coefficient is roughly set to 4. Since the ATM-dependent phosphorylation of p53 and ATM can be considered as enzyme-catalytic reactions, both the activation rate of p53 and the degradation rate of Mdm2 are assumed to depend on ATM level in a Michaelis-Menten form [14]. It is assumed that the $Mdm2_n$-dependent degradation rate of $p53^*$ is much smaller than that of p53 since Mdm2 shows a weaker binding to $p53^*$ than p53 [15]. The Mdm2-dependent p53 degradation is described in a Michaelis-Menten form since Mdm2 is a ligase promoting p53 degradation [21]. Considering the effect of Akt on the nuclear translocation of Mdm2 [22], it is assumed that Akt^* promotes the conversion from $Mdm2_c$ to $Mdm2_{cp}$ by phosphorylation, and only $Mdm2_{cp}$ can enter the nucleus to degrade p53. In addition, it is assumed that the activation rate of Akt is PIP3-dependent since PIP3 is required for the

activation of Akt by phosphorylation at the plasma membrane [23].

Cell fate decision module. Here we mainly characterize the role of p53 in regulating expression of downstream target genes and mediating cell fate decision. We classify p53* into p53 arrester and p53 killer according to its phosphorylation status and function. p53 arrester is the primarily phosphorylated p53 that mainly induces cell cycle arrest, while p53 killer refers to the further phosphorylated p53 (especially at Ser-46) that prefers to induce apoptosis [24]. The two proarrest gens, p21 and Wip1, are controlled by p53 arrester [25]. Moreover, p53 arrester also contributes to slow accumulation of p53DINP1 [26]. The three proapoptotic genes, p53DINP1, PTEN and p53AIP1, are mainly induced by p53 killer [24, 26, 27]. The conversion between p53 arrester and p53 killer is determined by Wip1 and p53DINP1: Wip1 inhibits the phosphorylation of p53 at Ser46 [28], while p53DINP1 promotes its phosphorylation [26]. p53AIP1 then results in cytochrome c release from the mitochondrial, which further activates caspase 3 to execute apoptosis [29]. A positive feedback loop between cytochrome c release and caspase 3 activation is considered in our model, which ensures the quick activation of caspase 3 [30]. It is noted that the induction of Wip1 by p53 arrester encloses the negative feedback loop between p53 arrester and ATM [31], while the induction of PTEN by p53 killer makes the positive feedback loop between p53 killer and PTEN closed [32]. Theses feedback loops may significantly influence the dynamics of the networks as well as the cellular outcome after DNA damage.

The dynamics of this module are characterized by Eqs. 15-23 in Supplemental method S2. The transition between p53 arrester and p53 killer is the key step for the selective expression of the target genes and p53-mediated cell fate decision (see Eqs. 15-18). The level of p53 killer is controlled by the levels of Wip1 and p53DINP1, and the level of p53 arrester is obtained by using the constraint condition (Eqs. 15-16) [24, 28, 33]. Wip1 expression is controlled by p53 arrester alone (Eq. 17). The expression of p53DINP1 is regulated by both forms of p53: p53 arrester induces it with a rather slow rate (k_{sdip11}) and p53 killer induces it with a fast rate (k_{sdinp12})(Eq. 18), satisfying $k_{\mathrm{sdip11}} \ll k_{\mathrm{sdinp12}}$ [24, 33]. p21 is only induced by p53 arrester (Eq. 20). The expression of PTEN and p53AIP1 is controlled by p53 killer (Eqs. 19,21) [24, 27]. It is assumed that the release rate of cytochrome c is p53AIP1-dependent, and this process is also promoted by caspase 3 [26, 30]. For the sake of simplicity, the intermediate effectors between cytochrome c release and caspase 3 activation, like Apaf-1 and caspase 9 [34], are not explicitly involved in the model. In addition, we did not consider the role of the Bcl-2 family proteins like PUMA, Bax and Bcl-2 in the model [35], and their role in apoptosis induction has been characterized by other models [36].

The robustness of p53 dynamics to parameter variation. In our model, some parameter values are based on experimental results and published models, while the others are estimated. Thus, it is necessary to investigate the robustness of network dynamics to parameter variations. While there are 87 parameters altogether in our model, we chose 12 parameters and increased/decreased their values by 15% around the standard values to explore their effects on p53 dynamics. The corresponding changes in the period of p53 pulses ($P\%$), the amplitude of p53 pulses ($A\%$), the steady-state level of p53 in the second phase ($L\%$), and the required number of p53 pulses preceding apoptosis induction ($n_{\rm ar}$) are listed in Supplemental Table S3.

In the table, the period of p53 pulses is rather sensitive to the synthesis of Wip1 ($k_{\rm swip1}$). The amplitude of p53 pulses is sensitive to the parameters related to the synthesis of p53 ($k_{\rm sp53}$), p53 activation ($k_{\rm acp530}$), and the synthesis of Wip1 ($k_{\rm swip1}$). The marked sensitivity of p53 pulsing to these parameters is consistent with the critical role of the p53-Wip1-ATM loop in generating p53 pulses. On the other hand, the pulse number $n_{\rm ar}$ is sensitive to the parameters involved in the conversion between p53 arrester and p53 killer, i.e., $k_{\rm swip1}$, $k_{\rm sdinp12}$, $k_{\rm sdinp13}$ and $k_{\rm p46}$. The variations in the above $n_{\rm ar}$-sensitive parameters even lead to sustained p53 pulses without the second phase. When the two-phase dynamics of p53 exist, the level of p53 in the second phase is sensitive to $k_{\rm sp53}$ and $k_{\rm acp530}$, which directly regulate the production and activation of p53. We have shown that the level of PTEN can significantly influence the dynamics of p53 in the second phase (see Fig. 6). Here the level of p53 in the second phase is not very sensitive to $k_{\rm spten}$ since the resultant value of $k_{\rm spten}$ is still far from the bifurcation point of 0.155. In addition, the sensitivity of p53 dynamics to other parameters can be inferred from this table. For example, the variation in $k_{\rm dp53}$ has an opposite effect on the mentioned quantities in the table compared with that in $k_{\rm sp53}$.

[1] Rothkamm K, Kruger I, Thompson LH, Lobrich M (2003) Pathways of DNA double-strand break repair during the mammalian cell cycle. *Mol Cell Biol* 23:5706-5715.

[2] Sengupta S, Harris CC (2005) p53: traffic cop at the crossroads of DNA repair and recombination. *Nat Rev Mol Cell Biol* 6:44-55.

[3] Tang W, Willers H, Powell SN (1999) p53 directly enhances rejoining of DNA double-strand breaks with cohesive ends in gamma-irradiated mouse fibroblasts. *Cancer Res* 59:2562-2565.

[4] Yang T NH, et al. (1997) p53 induced by ionizing radiation mediates DNA end-jointing activity, but not apoptosis of thyroid cells. *Oncogene* 14:1511-1519.

[5] Bill CA, Yu Y, Miselis NR, Little JB, Nickoloff JA (1997) A role for p53 in DNA end rejoining by human cell extracts. *Mutat Res* 385:21-29.

[6] Akyuz N, et al. (2002) DNA substrate dependence of p53-mediated regulation of double-strand break repair. *Mol Cell Biol* 22:6306-6317.

[7] Stewart RD (2001) Two-lesion kinetic model of double-strand break rejoining and cell killing. *Radiat Res* 156:365-378.

[8] Ma L, et al. (2005) A plausible model for the digital response of p53 to DNA damage. *Proc Natl Acad Sci USA* 102:14266-14271.

[9] Zhang X-P, Liu F, Cheng Z, Wang W (2009) Cell fate decision mediated by p53 pulses. *Proc Natl Acad Sci USA* 106:12245-12250.

[10] Zhang X-P, Liu F, Wang W (2010) Coordination between cell cycle progression and cell fate decision by the p53 and E2F1 pathways in response to DNA damage. *J Biol Chem* 285:31571-31580.

[11] Rothkamm K, Löbrich M (2003) Evidence for a lack of DNA double-strand break repair in human cells exposed to very low x-ray doses. *Proc Natl Acad Sci USA* 100:5057-5062.

[12] Bakkenist CJ, Kastan MB (2003) DNA damage activates ATM through intermolecular autophosphorylation and dimer dissociation. *Nature* 421:499-506.

[13] Shreeram S, et al. (2006) Wip1 phosphatase modulates ATM-dependent signaling pathways. *Mol Cell* 23:757-764.

[14] Kholodenko BN (2006) Cell-signalling dynamics in time and space. *Nat Rev Mol Cell Biol* 7:165-176.

[15] Prives C (1998) Signaling to p53: breaking the Mdm2-p53 circuit. *Cell* 95:5-8.

[16] Stommel JM, Wahl GM (2004) Accelerated MDM2 auto-degradation induced by DNA-damage kinases is required for p53 activation. *EMBO J* 23:1547-1556.

[17] Green DR, Kroemer G (2009) Cytoplasmic functions of the tumour suppressor p53. *Nature* 458:1127-1130.

[18] Pu T, Zhang X-P, Liu F, Wang W (2010) Coordination of the nuclear and cytoplasmic activities of p53 in response to DNA damage. *Biophys J* 99:1696-1705.

[19] Wu X, Bayle JH, Olson D, Levine AJ (1993) The p53-mdm2 autoregulatory feedback loop. *Genes Dev* 7:1126-1132.

[20] Jeffrey P, Gorina S, Pavletich N (1995) Crystal structure of the tetramerization domain of the p53 tumor suppressor at 1.7 angstroms. *Science* 267:1498-1502.

[21] Fang SY, Jensen JP, Ludwig RL, Vousden KH, Weissman AM (2000) Mdm2 is a ring finger-dependent ubiquitin protein ligase for itself and p53. *J Biol Chem* 275:8945-8951.

[22] Mayo LD, Donner DB (2001) A phosphatidylinositol 3-kinase/Akt pathway promotes translocation of Mdm2 from the cytoplasm to the nucleus. *Proc Natl Acad Sci USA* 98:11598-11603.

[23] Manning BD, Cantley LC (2007) AKT/PKB signaling: Navigating downstream. *Cell* 129:1261-1274.

[24] Oda K, et al. (2000) p53AIP1, a potential mediator of p53-dependent apoptosis, and its regulation by Ser-46-phosphorylated p53. *Cell* 102:849-862.

[25] Fiscella M, et al. (1997) Wip1, a novel human protein phosphatase that is induced in response to ionizing radiation in a p53-dependent manner. *Proc Natl Acad Sci USA* 94:6048-6053.

[26] Okamura S, et al. (2001) p53DINP1, a p53-inducible gene, regulates p53-dependent apoptosis. *Mol Cell* 8:85-94.

[27] Mayo LD, et al. (2005) Phosphorylation of human p53 at Serine 46 determines promoter selection and whether apoptosis is attenuated or amplified. *J Biol Chem* 280:25953-25959.

[28] Takekawa M, et al. (2000) p53-inducible Wip1 phosphatase mediates a negative feedback regulation of p38 MAPK-p53 signaling in response to UV radiation. *EMBO J* 19:6517-6526.

[29] Matsuda K, et al. (2002) p53AIP1 regulates the Mitochondrial apoptotic pathway. *Cancer Res* 62:2883-2889.

[30] Kirsch DG, et al. (1999) Caspase-3-dependent cleavage of Bcl-2 promotes release of cytochrome c. *J Biol Chem* 274:21155-21161.

[31] Batchelor E, Mock CS, Bhan I, Loewer A, Lahav G (2008) Recurrent initiation: A mechanism for triggering p53 pulses in response to DNA damage. *Mol Cell* 30:277-289.

[32] Wee KB, Aguda BD (2006) Akt versus p53 in a network of oncogenes and tumor suppressor genes regulating cell survival and death. *Biophys J* 91:857-865.

[33] Zhang TL, Brazhnik P, Tyson JJ (2007) Exploring mechanisms of the DNA-damage response - p53 pulses and their possible relevance to apoptosis. *Cell Cycle* 6:85-94.

[34] Malladi S, Challa-Malladi M, Fearnhead HO, Bratton SB (2009) The Apaf-1•procaspase-9 apoptosome complex functions as a proteolytic-based molecular timer. *EMBO J* 28:1916-1925.

[35] Youle RJ, Strasser A (2008) The BCL-2 protein family: opposing activities that mediate cell death. *Nat Rev Mol Cell Biol* 9:47-59.

[36] Bagci EZ, Vodovotz Y, Billiar TR, Ermentrout GB, Bahar I (2006) Bistability in apoptosis: roles of Bax, Bcl-2, and mitochondrial permeability transition pores. *Biophys J* 90:1546-1559.

Supplemental Method S2: Equations of the model

$$\frac{d[ATM_2]}{dt} = 0.5 * k_{dim} * [ATM]^2 - k_{undim} * [ATM_2] \quad (1)$$

$$\frac{d[ATM^*]}{dt} = k_{acatm} * n_c/(n_c + j_{nc}) * [ATM^*] * [ATM]/([ATM] + j_{acatm}) - k_{deatm} * (1 + [Wip1]) * [ATM^*]/([ATM^*] + j_{deatm}) \quad (2)$$

$$[ATM] = ATM_{tot} - 2 * [ATM_2] - [ATM^*] \quad (3)$$

$$k_{dmdm2n} = k_{dmdm2n0} + k_{dmdm2n1} * [ATM^*]/([ATM^*] + j_{atm}) \quad (4)$$

$$k_{acp53} = k_{acp531} * [ATM^*]/([ATM^*] + j_{atm}) \quad (5)$$

$$\frac{d[p53^*]}{dt} = k_{acp53} * [p53] - k_{dep53} * [p53^*] - k_{dp53s} * [Mdm2_n] * [p53^*]/(j_{1p53n} + [p53^*]) \quad (6)$$

$$\frac{d[p53]}{dt} = k_{sp53} - k_{dp53n} * [p53] - k_{dp53} * [Mdm2_n] * [p53]/(j_{1p53n} + [p53]) - k_{acp53} * [p53] + k_{dep53} * [p53^*] \quad (7)$$

$$\frac{d[Mdm2_c]}{dt} = k_{smdm20} + k_{smdm2} * [p53^*]^4/({j_{smdm2}}^4 + [p53^*]^4) - k_{dmdm2c} * [Mdm2_c] + k_{1mdm2s} * [Mdm2_{cp}]/(j_{1mdm2s} + [Mdm2_{cp}]) - k_{mdm2s} * [Mdm2_c] * [Akt^*]/(j_{mdm2s} + [Mdm2_c]) \quad (8)$$

$$\frac{d[Mdm2_{cp}]}{dt} = k_{mdm2s} * [Mdm2_c] * [Akt^*]/(j_{mdm2s} + [Mdm2_c]) - k_{1mdm2s} * [Mdm2_{cp}] /(j_{1mdm2s} + [Mdm2_{cp}]) - k_i * [Mdm2_{cp}] + k_o * [Mdm2_n] - k_{dmdm2c} * [Mdm2_{cp}] \quad (9)$$

$$\frac{d[Mdm2_n]}{dt} = k_i * [Mdm2_{cp}] - k_o * [Mdm2_n] - k_{dmdm2n} * [Mdm2_n] \quad (10)$$

$$\frac{d[Akt^*]}{dt} = k_{acakt} * [PIP3] * [Akt]/(j_{acakt} + [Akt]) - k_{deakt} * [Akt^*]/(j_{deakt} + [Akt^*]) \quad (11)$$

$$[Akt] = Akt_{tot} - [Akt^*] \quad (12)$$

$$\frac{d[PIP3]}{dt} = k_{p2} * [PIP2]/([PIP2] + j_{p2}) - k_{p3} * [PTEN] * [PIP3]/([PIP3] + j_{p3}) \quad (13)$$

$$[PIP2] = PIP_{tot} - [PIP3] \quad (14)$$

$$\frac{d[p53\ killer]}{dt} = k_{p46} * [p53DINP1] * [p53\ arrester]/(j_{p46} + [p53\ arrester]) - k_{dp46} * [Wip1] * [p53\ killer]/(j_{dp46} + [p53\ killer]) \quad (15)$$

$$[p53\ arrester] = [p53^*] - [p53\ killer] \quad (16)$$

$$\frac{d[\text{Wip1}]}{dt} = k_{swip10} + k_{swip1} * [\text{p53 arrester}]^3/(j_{swip1}{}^3 + [\text{p53 arrester}]^3) - k_{dwip1} * [\text{Wip1}] \quad (17)$$

$$\frac{d[\text{p53DINP1}]}{dt} = k_{sdinp10} + k_{sdinp11} * [\text{p53 arrester}]^3/(j_{sdinp11}{}^3 + [\text{p53 arrester}]^3) + k_{sdinp12} * [\text{p53 killer}]^3/(j_{sdinp12}{}^3 + [\text{p53 killer}]^3) - k_{ddinp1} * [\text{p53DINP1}] \quad (18)$$

$$\frac{d[\text{PTEN}]}{dt} = k_{spten0} + k_{spten} * [\text{p53 killer}]^3/([\text{p53 killer}]^3 + j_{spten}{}^3) - k_{dpten} * [\text{PTEN}] \quad (19)$$

$$\frac{d[\text{p21}]}{dt} = k_{sp210} + k_{sp21} * [\text{p53 arrester}]^3/(j_{sp21}{}^3 + [\text{p53 arrester}]^3) - k_{dp21} * [\text{p21}] \quad (20)$$

$$\frac{d[\text{p53AIP1}]}{dt} = k_{saip10} + k_{saip1} * [\text{p53 killer}]^3/(j_{saip1}{}^3 + [\text{p53 killer}]^3) - k_{daip1} * [\text{p53AIP1}] \quad (21)$$

$$\frac{d[\text{CytoC}]}{dt} = (k_{accytoc0} + k_{accytoc1} * [\text{p53AIP1}] * [\text{Casp3}]^4/([\text{Casp3}]^4 + j_{casp3}{}^4)) * (\text{CytoC}_{tot} - [\text{CytoC}]) - k_{decytoc} * [\text{CytoC}] \quad (22)$$

$$\frac{d[\text{Casp3}]}{dt} = (k_{accasp30} + k_{accasp31} * [\text{Cytc}]^4/([\text{Cytc}]^4 + j_{cytoc}{}^4)) * (\text{Casp3}_{tot} - [\text{Casp3}]) - k_{decasp3} * [\text{Casp3}] \quad (23)$$

Supplemental Table S1: Variables of the model

Variable	Description	Initial values
[ATM_2]	Concentration of ATM dimer	2.17
[ATM^*]	Concentration of active ATM monomer	0
[p53]	Concentration of inactive p53	0.8
[$p53^*$]	Concentration of active p53	0.0
[$Mdm2_c$]	Concentration of cytoplasmic Mdm2	0.01
[$Mdm2_{cp}$]	Concentration of phosphorylated cytoplasmic Mdm2	0.4
[$Mdm2_n$]	Concentration of nuclear Mdm2	0.26
[Akt]	Concentration of inactive Akt	0.06
[Akt^*]	Concentration of active Akt	0.94
[PIP2]	Concentration of PIP2	0.11
[PIP3]	Concentration of PIP3	0.89
[PTEN]	Concentration of PTEN	0.1
[p53 arrester]	Concentration of primarily phosphorylated p53	0.0
[p53 killer]	Concentration of further phosphorylated p53 at Ser46	0.0
[p21]	Concentration of p21	0.1
[Wip1]	Concentration of wild-type p53 induced protein 1	0.2
[p53DINP1]	Concentration of p53-dependent damage-inducible protein 1	0.0
[p53AIP1]	Concentration of p53-regulated apoptosis-inducing protein 1	0.1
[CytoC]	Concentration of cytochrome c	0.06
[Casp3]	Concentration of active caspase 3	0.05

Supplemental Table S2: Parameters of the model

Rate Constant	Description	Value	Reference
n_{RPT}	Number of repair proteins	20	[8]
k_{fb1}	Association rate of repair proteins in fast kinetics	1.3	[7, 8]
k_{fb2}	Association rate of repair proteins in slow kinetics	0.13	[7, 8]
k_{rb1}	Dissociation rate of repair proteins in fast kinetics	0.3	[7, 8]
k_{rb2}	Dissociation rate of repair proteins in slow kinetics	0.03	[7, 8]
k_{fix1}	DSB ligation rate in fast kinetics	0.02	[7, 8]
k_{fix2}	DSB ligation rate in slow kinetics	0.002	[7, 8]
k_{cross}	DSB binary mismatch rate	0.0007	[7, 8]
k_{dim}	ATM dimerization rate	10	[8]
k_{undim}	ATM undimerization rate	1	[8]
k_{acatm}	ATM activation rate	2	[8]
k_{deatm}	ATM inactivation rate	1.3	[8]
j_{acatm}	Michaelis constant of ATM activation	1	[8]
j_{deatm}	Michaelis constant of ATM* inactivation	2.3	[8]
j_{nc}	Threshold number of DSBC for ATM activation	1	[8]
ATM_{tot}	The total concentration of all forms of ATM	5	[8]
k_{dmdm2n0}	Basel degradation rate of Mdm2	0.003	[8]
k_{dmdm2n1}	ATM-dependent degradation rate of Mdm2	0.05	[8]
j_{atm}	Michaelis constant of ATM* as a kinase	1	Estimated
k_{acp531}	ATM-dependent activation rate of p53	0.2	[8]
k_{dep53}	Deactivation rate of p53	0.1	[8, 32]
k_{dp53s}	Mdm2-dependent degradation rate of p53*	0.01	[8]
k_{sp53}	Production rate of p53	0.2	[8, 32]
k_{dp53n}	Basal degradation rate of p53	0.05	[8, 32]
k_{dp53}	Mdm2-dependent degradation rate of p53	0.7	[8]
j_{1p53n}	Michaelis constant of Mdm2-dependent p53 degradation	0.1	Estimated
k_{smdm20}	Basal production rate of Mdm2	0.002	[8]
k_{smdm2}	p53-dependent production rate of Mdm2	0.024	[8]
j_{smdm2}	Michaelis constant of p53-dependent Mdm2 production	1	Estimated
k_{dmdm2c}	Degradation rate of cytoplasmic Mdm2	0.003	[32]
k_{1mdm2s}	Dephosphorylation rate of cytoplasmic Mdm2	0.3	[32]
j_{1mdm2s}	Michaelis constant of Mdm2 dephosphorylation	0.1	[32]
k_{mdm2s}	Akt-dependent phosphorylation rate of cytoplasmic Mdm2	8	[32]
j_{mdm2s}	Michaelis constant of Akt-dependent Mdm2 dephosphorylation	0.3	[32]

Supplemental Table S2-Continued

k_{i}	Nuclear import rate of $\mathrm{Mdm2_{cp}}$	0.06	Estimated
k_{o}	Nuclear export rate of $\mathrm{Mdm2_{n}}$	0.09	Estimated
k_{acakt}	Phosphorylation rate of Akt	0.25	[32]
j_{acakt}	Michaelis constant of Akt phosphorylation	0.1	[32]
k_{deakt}	Dephosphorylation rate of Akt*	0.1	[32]
j_{deakt}	Michaelis constant of Akt* dephosphorylation	0.2	[32]
k_{p2}	Phosphorylation rate of PIP2	0.1	[32]
j_{p2}	Michaelis constant of PIP2 phosphorylation	0.2	[32]
k_{p3}	PTEN-dependent dephosphorylation rate of PIP3	0.5	[32]
j_{p3}	Michaelis constant of PIP3 dephosphorylation	0.4	[32]
PIP_{tot}	Total concentration of PIP2 and PIP3	1	[8]
Akt_{tot}	Total concentration of all forms of of Akt	1	[32]
k_{p46}	Rate constant of p53 arrester phosphorylation	0.6	Estimated
j_{p46}	Michaelis constant of p53 arrester phosphorylation	0.5	Estimated
k_{dp46}	Rate constant of p53 killer dephosphorylation	0.3	Estimated
j_{dp46}	Michaelis constant of p53 killer dephosphorylation	0.2	Estimated
k_{swip10}	Basal induction rate of Wip1	0.01	Estimated
k_{swip1}	p53 arrester-dependent production rate of Wip1	0.09	Estimated
j_{swip1}	Michaelis constant of p53 arrester-dependent Wip1 production	0.5	Estimated
k_{dwip1}	Degradation rate of Wip1	0.05	Estimated
k_{sdinp10}	Basal induction rate of p53DINP1	0.001	[33]
k_{sdinp11}	p53 arrester-dependent production rate of p53DINP1	0.01	[33]
j_{sdinp11}	Michaelis constant of p53 arrester-dependent p53DINP1 production	0.7	[33]
k_{sdinp12}	p53 killer and E2F1-dependent production rate of p53DINP1	0.07	[33]
j_{sdinp12}	Michaelis constant of p53 killer-dependent p53DINP1 production	0.3	[33]
k_{ddinp1}	Degradation rate of p53DINP1	0.01	Estimated
k_{spten0}	Basal induction rate of PTEN	0.01	Estimated
k_{spten}	p53 killer-dependent production rate of PTEN	0.5	Estimated
j_{spten}	Michaelis constant of p53 arrester-dependent PTEN production	1	Estimated
k_{dpten}	Degradation rate of PTEN	0.1	Estimated
k_{sp210}	Basal induction rate of p21	0.01	Estimated
k_{sp21}	p53 arrester-dependent production rate of p21	0.2	Estimated
j_{sp21}	Michaelis constant of p53 arrester-dependent p21 production	0.6	Estimated
k_{dp21}	Degradation rate of p21	0.1	Estimated

Supplemental Table S2-Continued

k_{saip10}	Basal induction rate of p53AIP1	0.01	Estimated
k_{saip1}	p53 killer dependent production rate of p53AIP1	0.32	Estimated
j_{saip1}	Michaelis constant of p53 killer dependent p53AIP1 production	1.5	Estimated
k_{daip1}	Degradation rate of p53AIP1	0.1	Estimated
k_{accytoc0}	Basal release rate of mitochondrial cytochrome c	0.001	Estimated
k_{accytoc1}	p53AIP1-dependent release rate of mitochondrial cytochrome c	0.9	Estimated
j_{casp3}	Michaelis constant of caspase 3-dependent cytochrome c release	0.5	Estimated
k_{decytoc}	Mitochondrial influx rate of cytochrome c	0.05	Estimated
$CytoC_{\mathrm{tot}}$	Total concentration of cytochrome c	3	Estimated
$Casp3_{\mathrm{tot}}$	Total concentration of caspase 3	3	Estimated
k_{accasp30}	Basal activation rate of caspase 3	0.001	Estimated
k_{accasp31}	Activation rate of caspase 3	0.9	Estimated
j_{cytoc}	Michaelis constant of cytochrome c dependent caspase 3 activation	0.5	Estimated
k_{decasp3}	Inactivation rate of caspase 3	0.07	Estimated

Supplemental Table S3: Robustness of p53 dynamics to parameter variations

	+15%				-15%			
Parameter	P%	A%	n_{ar}	L%	P%	A%	n_{ar}	L%
k_{acp530}	1.5	4.5	4	15.0	-1.6	-4.5	4	**-15.0**
k_{sp53}	1.3	**13.4**	4	**16.9**	-4.6	**-11.2**	3	-17.0
k_{smdm2}	-1.5	-3.0	4	-0.1	1.4	3.7	4	0.1
k_{mdm2s}	0.0	0.4	4	-3.4	0.0	0.7	4	3.1
k_{i}	-0.4	-1.5	4	2.4	0.7	3.0	4	2.1
k_{acakt}	0.0	0.3	4	-4.3	0.0	0.4	4	3.4
k_{p2}	0.0	0.4	4	-4.6	0.0	0.4	4	3.6
k_{p46}	-2.6	3.0	**1**	0.0	2.2	-0.7	-	-
k_{swip1}	**8.8**	-3.7	-	-	**-11.3**	7.5	**1**	0.0
k_{sdinp11}	-1.7	0.0	**2**	0.0	1.6	0.0	-	-
k_{sdinp12}	-0.4	0.7	3	0.0	0.3	0.0	-	-
k_{spten}	0.0	0.4	4	3.1	0.0	0.4	4	-5.3

Note: "-" indicates the disappearance of p53 pulses or steady states of p53 in the second phase. Each bold number means that the quantity is very sensitive to the variation in the corresponding parameter.

Supplemental Figures

Figure legends

Supplemental Figure S1: Time courses of the levels of ATM* and Wip1 for three individual cells at $D_{\mathrm{IR}} = 5$ Gy.

Supplemental Figure S2: The effect of the p53-inducible synthesis rate of Mdm2, k_{smdm2}, on p53 oscillations. (A) p53 oscillations obtained from our model with $k_{\mathrm{smdm2}} = 0$ (black) and $k_{\mathrm{smdm2}} = 0.3$ (red). (B) p53 oscillations obtained from the model by Batchelor *et al.* [31] with $k_{\mathrm{smdm2}} = 0$.

Supplemental Figure S3: Time courses of the levels of p53 arrester, p53 killer, p21, Wip1, PTEN, p53AIP1 and Casp3 at $D_{\mathrm{IR}} = 3$ Gy (A) or 5 Gy (B).

Supplemental Figure S4: Time courses of the levels of p53 arrester, p53 killer and Casp3 in three individual cells at $D_{\mathrm{IR}} = 5$ Gy.

Supplemental Figure S5: The link between a sequential predominance of distinct feedback loops and p53-mediated cellular outcomes.

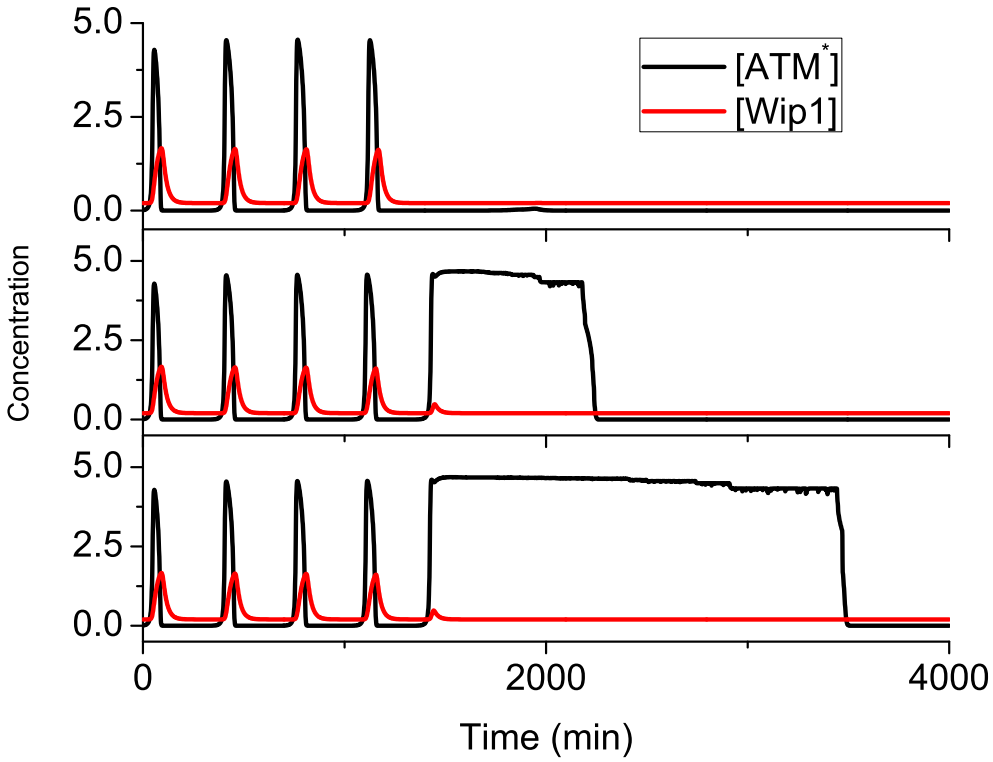

Supplemental Figure S1

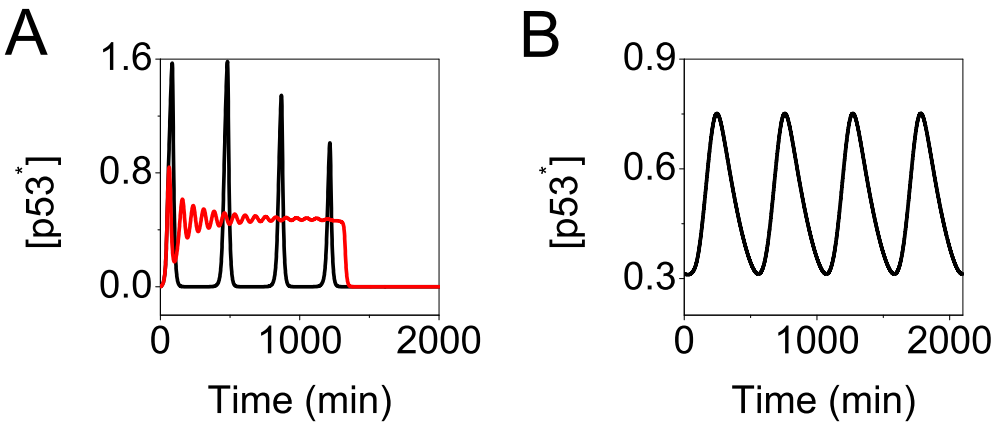

Supplemental Figure S2

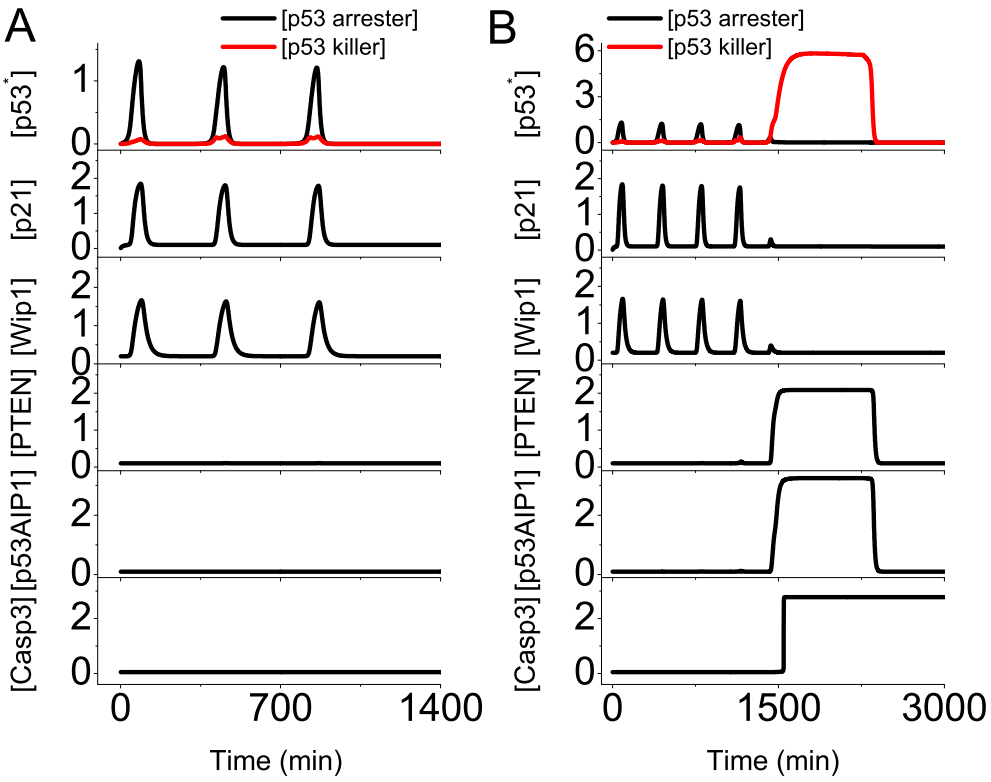

Supplemental Figure S3

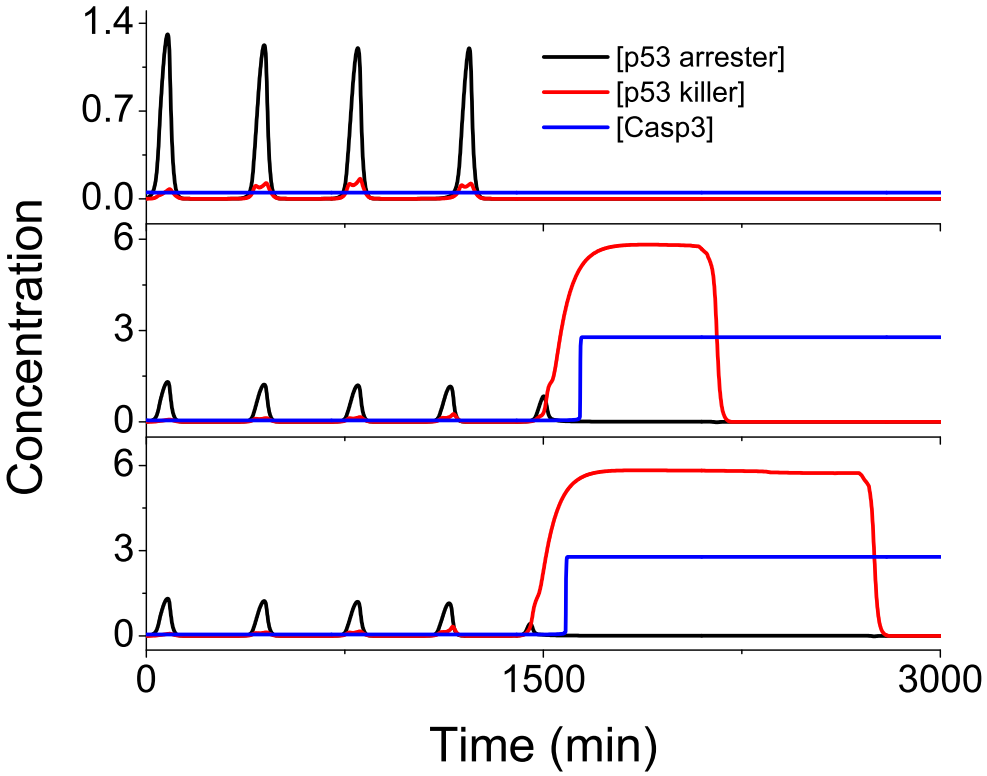

Supplemental Figure S4

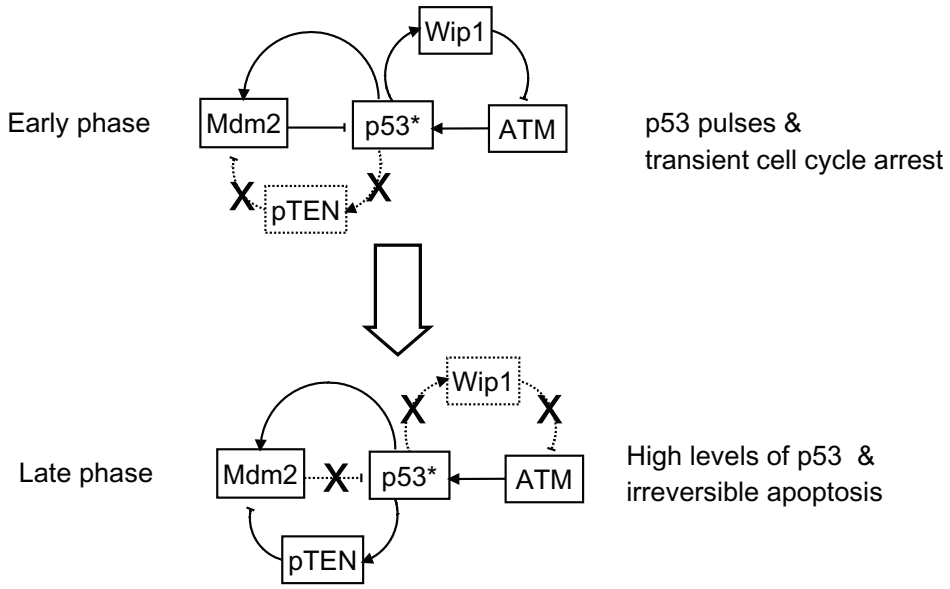

Supplemental Figure S5